JMEPEG
https://doi.org/10.1007/s11665-024-09829-1

1059-9495/$19.00

ORIGINAL RESEARCH ARTICLE

Effect of Vanadium Content on Microstructure and Wear Behavior of Fe-Cr-Mn-C Surfacing Alloys

Minghui Zhuang, Qicong Liu, Xiaoxia Li, Hui Yang, Yanan Ren, Xuyou Liu, Yudong Yan, and Zhen Ma

Submitted: 17 January 2024 / Revised: 4 May 2024 / Accepted: 18 May 2024

To address the brittleness issue inherent in Fe-Cr-C wear-resistant surfacing alloys and enhance their wear resistance, this study comprehensively investigates the influence of vanadium on the microstructure, impact toughness, and wear performance of Fe-Cr-Mn-C alloys. Employing an array of characterization techniques, including metallographic microscope (OM), x-ray diffraction, field emission scanning electron microscopy, energy-dispersive spectroscopy, impact testing, hardness testing, and abrasive wear testing, this research delineates the role of vanadium addition. The experimental results reveal that vanadium modifies the microstructural features of the alloys. A minor addition of vanadium preferentially dissolves in the primary M_7C_3 carbides, whereas a higher concentration of vanadium fosters the crystallization of these primary carbides and the formation of secondary hard particles, notably VC, thereby refining the carbide grains. The impact toughness exhibits a nonlinear response to increasing vanadium content, initially decreasing, and then subsequently improving. Notably, the alloy with 14.11 wt.% Mn and 7.11 wt.% V achieves the peak impact toughness at 30.00 J/cm^2. Further, the analyses of hardness and two-body abrasive wear indicate a similar trend: performance deteriorates initially with the addition of vanadium but improves with higher concentrations. The optimal mechanical properties are attained when the alloy composition includes 14.11 wt.% Mn and 7.11 wt.% V, where the hardness reaches up to 55.9 HRC and the wear loss under a 24 N load is minimized to 30.6 mg. This study underscores the nuanced effects of vanadium in enhancing the durability and mechanical robustness of Fe-Cr-Mn-C surfacing alloys.

Keywords Fe-Cr-Mn-V-C alloy, microscopic structure, plasma surfacing, wear resistance

1. Introduction

Abrasive wear poses a significant challenge in various industrial sectors, including iron and steel metallurgy, mining, and cement production, often leading to the premature failure of components. Enhancing the wear resistance of these components or reinforcing parts prone to failure extends the lifespan of the equipment and augments the economic output of enterprises (Ref 1-4). Consequently, the development of materials with superior wear resistance and mechanical properties remains a central focus among materials scientists.

High-chromium cast iron (HCCI), containing 12-30% Cr and 2.0-4.3% C, is extensively utilized for its exceptional wear resistance in abrasive environments. The outstanding wear resistance of HCCI is attributed to the high volume fraction of hard M_7C_3 carbides (hardness of 1300-1800 HV) embedded in its matrix structure (Ref 5-7). Despite its advantages, the application of HCCI is limited by the brittleness of its coarse primary M_7C_3 carbides, which are susceptible to cracking, breaking, and delaminating under-high stress conditions. This vulnerability results in severe wear of the surfacing alloy layer and a reduction in the service life of components. Therefore, developing HCCI variants that combine high hardness with satisfactory toughness is crucial for enhancing their wear resistance and operational longevity (Ref 8-10). This advancement holds significant implications for improving the durability and efficiency of industrial equipment.

To enhance operational performance under demanding conditions, various strategies such as heat treatment (Ref 11, 12), alloying (Ref 13, 14), and other techniques can be employed to improve the anti-wear characteristics of materials. Specifically, Guo et al. (Ref 15) investigated the impact of different heat treatment procedures on the microstructure and properties of high-chromium cast iron used in rolls. Their findings indicate that quenching and tempering significantly enhance both the impact toughness and wear resistance of HCCI. Nonetheless, such heat treatments are associated with challenges including the increase in carbide content, propagation of cracks, and coarsening of the microstructure. Moreover, for large-scale engineering equipment, it has been observed that post-surfacing repair heat treatment does not effectively enhance wear resistance. This limitation suggests the need for alternative methods or improvements in heat treatment techniques to address the specific wear challenges in large engineered systems, ensuring durability and reliability in industrial applications.

Minghui Zhuang, Qicong Liu, Hui Yang, Yudong Yan, and **Zhen Ma**, School of Materials Science and Engineering, Jiamusi University, Jiamusi 154007, People's Republic of China; **Xiaoxia Li**, College of Science, Jiamusi University, Jiamusi 154007, People's Republic of China; **Yanan Ren**, College of Foreign Languages, Jiamusi University, Jiamusi 154007, People's Republic of China; and **Xuyou Liu**, Binzhou Inspection and Testing Center, Binzhou 256600, People's Republic of China. Contact e-mail: jmsdxmz@163.com.

Published online: 22 July 2024

Alloying is currently recognized as an effective strategy to enhance the wear resistance of high-chromium cast iron. With the rapid advancements in surfacing remanufacturing technology, the technique of alloy modification has undergone extensive research and widespread application. Research indicates that alloying treatments refine the primary M_7C_3 carbides in high-chromium cast iron, significantly improving its wear resistance (Ref 16). There are noteworthy findings regarding the refinement of primary M_7C_3 carbides and the modulation of wear resistance in high-chromium cast iron through alloying strategies. Liu et al. (Ref 17) explored the influence of Ti on the microstructure and wear properties of Fe-Cr-C wear-resistant surfacing alloys. Their studies reveal that the addition of Ti promotes the crystallization of TiC, which serves as a heterogeneous nucleation core for primary M_7C_3 carbides, facilitating grain refinement. This addition leads to enhanced hardness and wear resistance in the surfacing alloy layer. Furthermore, vanadium carbides (VxCy), with their higher hardness compared to M_3C and M_7C_3 carbides and low solubility in molten iron, contribute to increased interfacial tension by segregating on the surface of "VC/melt". This adjustment in surface tension reduces the differential growth rates of VC crystals, allowing them to grow spherically. The spherical growth of VC carbides reduces stress concentration, thereby improving the mechanical properties and wear resistance of the high-chromium cast iron surfacing alloy layer (Ref 18). Additionally, VC carbides also act as heterogeneous nucleation sites for primary M_7C_3 carbides, refining them further and enhancing the wear resistance of the high-chromium cast iron. In this context, vanadium is regarded as a highly promising alloying element (Ref 19, 20). Efremenko et al. (Ref 21) examined the effects of varying concentrations of vanadium (5-10 wt.%) and chromium (0-9 wt.%) on the microstructure and hardness of V-Cr-Mn-Ni white cast iron. Their results demonstrate that the inclusion of vanadium and chromium not only increases the total carbide content and austenite in the matrix but also significantly boosts the hardness and wear resistance of the white cast iron.

Enhancing the performance of surfacing alloy layers through the singular modulation of primary carbides is inherently limited, particularly as such modulation does not typically influence the matrix structure. However, tailoring the matrix structure can mitigate stress during both the welding and wear processes, thereby enhancing the crack resistance of the surfacing alloy layer. By reducing the propensity for fracture and spalling, significant improvements in wear resistance can be achieved. Previously, our research group explored the addition of Mn to the Fe-B wear-resistant surfacing alloy layer. This alloying strategy aimed to transition the matrix from ferrite or martensite to austenite. Austenite is known for its excellent plasticity, which helps to alleviate the brittleness typical of Fe-B wear-resistant surfacing alloys, diminishes the occurrence of crushing, and ultimately enhances wear resistance. Moreover, under conditions of high stress or impact, austenite undergoes a transformation into martensite, a phase change that further augments the wear resistance of the surfacing alloy layer (Ref 22). Consequently, manganese has emerged as the preferred alloying element for regulating the matrix phase, providing a robust strategy for improving the mechanical properties and durability of surfacing alloys.

Numerous studies both domestically and internationally have focused on the modification of primary carbide structures and the regulation of the matrix phase through heat treatment to enhance the properties of high-chromium cast iron. However, research on the synergistic regulation of the primary phase, eutectic carbide, and matrix phase remains relatively sparse. In this study, we introduce Mn and V to the wear-resistant surfacing alloy layer of the high-chromium cast iron system, aiming to achieve a synergistic adjustment of both the matrix and primary phases through alloying. We systematically investigate the impact of varying concentrations of Mn and V on the microstructure and properties of the wear-resistant surfacing alloy layer in the high-chromium cast iron system, exploring how these alterations influence overall material performance. This comprehensive analysis contributes to a deeper understanding of the intricate interactions within the alloy system, potentially leading to more effective strategies for enhancing wear resistance in industrial applications.

2. Experimental Procedure

2.1 Surfacing Process

In this study, we employed plasma surfacing to deposit a wear-resistant alloy layer on a steel substrate using Q235 as the base material. The Q235 steel plate measured 150 mm × 100 mm × 10 mm, with its chemical composition detailed in Table 1. Prior to surfacing, surface preparation was performed using an angle grinder to remove any rust. The optimized parameters for the plasma surfacing experiment are presented in Table 2. The alloy powder utilized in this experiment was procured from Jinzhou Co., Ltd. It had a particle size of 100 mesh, and its chemical composition is provided in Table 3. To ensure homogeneity and optimal condition for surfacing, the

Table 1 Chemical compositions of the Q235 substrate (wt.%)

Elements	C	Mn	Si	P	S	Fe
Content	< 0.150	< 0.500	< 0.300	< 0.025	< 0.040	bal.

Table 2 Surfacing process parameters

Voltage, U/V	Current, I/A	Ion flow, L/min	Protective air flow, L/min	Powder air flow, L/min	Swing speed, m/min
25	130	3	6	4	11

Table 3 Chemical composition of alloy powder (wt.%)

Alloy powers	Cr	Mn	V	Si	C	P	S	Fe
High-carbon ferrochrome powders	68.64	…	…	0.50	8.51	0.028	0.028	bal.
High-carbon ferromanganese powder	…	75.76	…	0.51	6.73	0.137	0.015	bal.
Ferrovanadium powder	…	…	50.40	1.00	0.096	0.041	0.012	bal.
Ferrosilicon powder	…	…	…	72.40	0.015	0.034	0.016	bal.
Reduced iron powder	…	0.40	…	0.15	0.05	0.025	0.030	bal.

Table 4 Chemical compositions of the surfacing alloy (wt.%)

Sample No.	Cr	Mn	V	Si	C	P	S	Fe
Mn2-V0	18.22	2.01	…	1.16	1.98	0.057	0.022	bal.
Mn14-V0	27.12	14.16	…	1.12	3.52	0.056	0.024	bal.
Mn14-V2	26.98	14.22	2.03	1.28	3.44	0.062	0.018	bal.
Mn14-V5	27.05	14.08	4.60	1.16	3.50	0.078	0.022	bal.
Mn14-V7	27.20	14.11	7.11	1.18	3.41	0.069	0.016	bal.

alloy powder was subjected to mixing for 0.5 h, followed by drying at 150 °C for 2 h. We designed a series of Fe-Cr-C wear-resistant surfacing alloy layers with varying contents of Mn and V. The chemical compositions of the surfacing alloy layers with different Mn and V contents were quantitatively analyzed using a direct-reading spectrometer, with the results detailed in Table 4. This methodical approach allowed for precise control over the alloying elements, facilitating a comprehensive investigation into their effects on the properties of the surfacing alloy layer.

2.2 Microstructure Characterization

In this study, samples measuring 10 mm × 10 mm × 10 mm were excised from the surfacing alloy layer using wire electrical discharge machining. The top and side surfaces of these samples were sequentially ground using SiC sandpaper ranging from coarse (#240) to fine (#2000) grits. Subsequent polishing was performed using diamond spray polishing agents, followed by etching with aqua regia to prepare the samples for microstructural analysis. The phase composition of the treated samples was investigated using x-ray diffraction (XRD; d8 Advance, Bruker AXS, Germany), employing Cu Kα radiation. The scan covered a range from 20° to 90° at a step rate of 2°/min. The microstructure and carbide morphology were examined using a Zeiss metallographic microscope (OM; Axio Observer, Carl Zeiss Inc., Germany) and a field emission scanning electron microscope (SEM; JSM-7800F, JEOL Ltd, Tokyo, Japan) equipped with backscattered electron imaging (BSE). Elemental content and distribution within the surfacing alloy layer samples were analyzed using an x-ray energy-dispersive spectrometer (EDS; Oxford X-maxn, Oxford Instruments, London, UK). Furthermore, electron backscatter diffraction (EBSD; NordlysMax2, Oxford Instruments, UK) was utilized to assess the phase composition and grain growth orientation. The EBSD measurements were conducted under the following conditions: an acceleration voltage of 20 kV, an acquisition speed of 10 Hz, a sample inclination angle of 70°, a working distance of 20.2 mm, and a scanning step size of 0.3 μm. This comprehensive suite of analytical techniques provided a detailed insight into the structural and compositional nuances of the surfacing alloy layers.

2.3 Mechanical Property Measurements

Following the grinding and polishing of the surfacing alloy layer, the macroscopic hardness was evaluated using a Rockwell hardness tester (HR-150A, Laizhou Testing Machine Diamond Tool Factory, Shandong). The testing parameters included a loading force of 150 kgf and a loading duration of 10 s, with hardness values averaged over five distinct points for each sample. Additionally, the microhardness of various phases within the microstructure on the side of the surfacing alloy layer was determined using a microhardness tester (HMV-2 T, Shimadzu, Japan). This tester applied a force of 50 gf and maintained it for 15 s per measurement. Impact toughness was assessed for samples with varying contents of manganese and vanadium using a JB30A pendulum impact tester at room temperature. The configuration of the impact specimens is depicted in Fig. 1. The morphology of the impact fractures was subsequently examined using a field emission scanning electron microscope (SEM). The wear properties of the surfacing alloy layer were analyzed using a twin abrasive wear tester (ML-100, Kehua Testing Machine Manufacturing Co., Ltd., China) at room temperature. The test samples were cylindrical, measuring Φ4 mm × 15 mm. Abrasion testing involved 180 mesh brown corundum sandpaper, with a loading force of 24 N, a turntable rotational speed of 60 r/min, and a stroke length of 75 m. The post-wear analysis included weighing the wear samples on an electronic balance accurate to 0.1 mg and examining the worn surface morphology using field emission SEM. This multifaceted approach provided a comprehensive evaluation of the mechanical properties and wear resistance of the surfacing alloy layers.

3. Results and Discussion

3.1 Phase Analysis

To elucidate the impact of varying manganese and vanadium contents on the phase composition of high-chromium cast iron surfacing alloy layers, tests were conducted on sections perpendicular to the surface of these layers. The findings are illustrated in Fig. 2. In the Mn2-V0 samples, which contain no vanadium and very low manganese, the phase composition predominantly includes ferrite and $(Cr, Fe)_7C_3$. An increase in manganese content induces a transformation of the matrix phase to austenite, accompanied by the emergence of a new diffraction peak for the $(Cr, Fe)_7C_3$ phase at a diffraction angle of 39.2° and an intensified peak at 44.4°. Comparison with the Joint Committee on Powder Diffraction Standards (JCPDS) 05-0720 shows that the $(Cr, Fe)_7C_3$ diffraction peaks align perfectly in intensity and position with the standard diffraction data. However, the γ-Fe peaks exhibit a rightward shift, as per standard PDF card 88-2324, indicative of the lattice distortion due to the substitutional solution of Mn atoms in Fe, leading to decreased crystal plane spacing and increased diffraction angles (Ref 23). Upon further alloying with vanadium, while no new phase diffraction peaks were observed, there was a notable increase in the intensity and quantity of $(Cr, Fe)_7C_3$ peaks.

This analysis suggests that manganese, as a stable austenitizing agent, effectively converts the matrix from ferrite to austenite. Concurrently, increasing manganese levels results in a higher volume fraction of $(Cr, Fe)_7C_3$ in the surfacing alloy layer. The primary role of added vanadium appears to be in enhancing the formation of $(Cr, Fe)_7C_3$ carbides, reinforcing the phase structure of the alloy.

3.2 Microstructure

Figure 3 displays the microstructural morphology of surfacing alloy layers with varying manganese contents, without the addition of vanadium. In alloys with low manganese content, Mn primarily acts alongside silicon to remove oxygen from the molten pool during the welding process, and it seldom contributes to the development of the microstructure (Ref 24). The microstructure of the Mn2-V0 sample predominantly consists of α-Fe dendrites and intergranular $(Cr, Fe)_7C_3$ carbides, characteristic of a typical hypoeutectic high-chromium cast iron. For the Mn14-V0 sample, which contains 14.16 wt.% manganese, the microstructure features a hexagonal block and small granular intergranular structures. According to XRD results and prior studies (Ref 25), the hexagonal block structure is identified as primary carbide M_7C_3 (M = Cr, Fe, Mn), and the eutectic structure consists of M_7C_3 + γ-Fe, typifying a hypereutectic high-chromium cast iron configuration. The transition from a hypoeutectic to a hypereutectic structure in the surfacing alloy layer is predominantly due to the addition of manganese. During the welding process, the alloy powder in the sample without added Mn exhibits significant splashing and poor wettability. The introduction of Mn enhances the wettability of the surfacing alloy layer, allowing more alloy powder to dissolve. Direct reading spectrometry reveals that the addition of Mn promotes greater dissolution of alloy elements such as Cr and C in the molten pool, a crucial factor in transitioning from a hypoeutectic to a hypereutectic structure. Furthermore, the addition of manganese shifts the eutectic point of the Fe-Cr-C alloy to the left, enabling the formation of eutectic or hypereutectic structures under constant Cr and C levels. The hexagonal block M_7C_3 carbides in the hypereutectic structure, known for their high hardness, impart enhanced wear resistance to the surfacing alloy layer (Ref 26).

To elucidate the impact of vanadium addition on the microstructure of Fe-Cr-Mn-C wear-resistant surfacing alloy layers, the morphologies were examined using the metallographic and scanning electron microscopy. The observations are documented in Fig. 4. In the Mn14-V0 sample, hexagonal block carbides exhibit a cross-sectional width of approximately 20-30 μm and a longitudinal dimension of about 100-200 μm, constituting around 60% of the volume fraction. The eutectic structure consists of irregular, small granular M_7C_3 + γ-Fe,

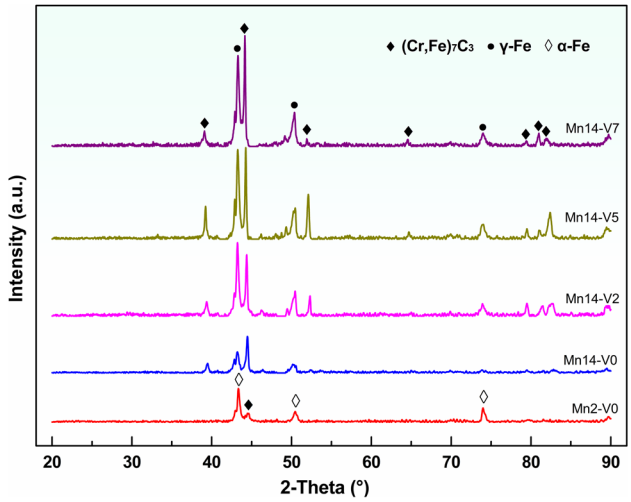

Fig. 2 XRD diffraction patterns of surfacing alloy layers with different manganese and vanadium contents

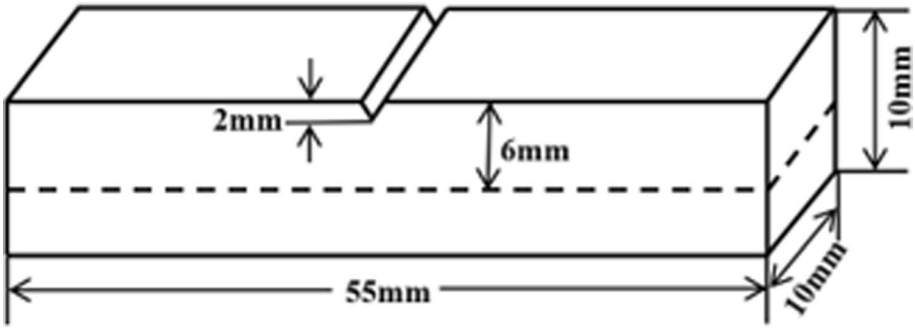

Fig. 1 Schematic diagram of impact sample size

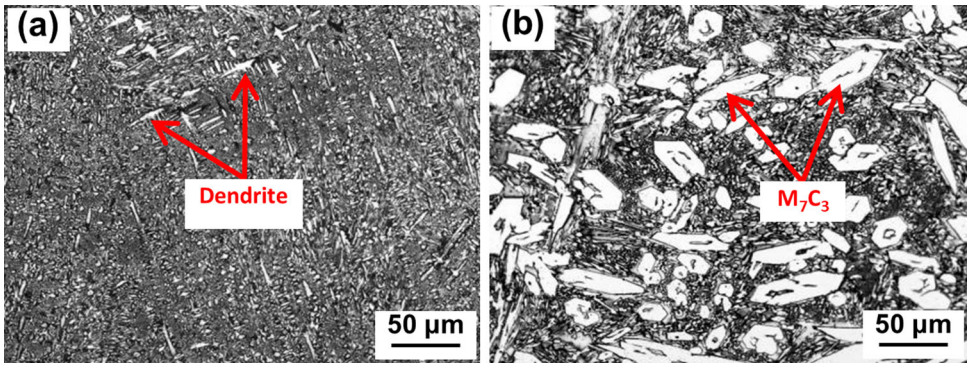

Fig. 3 Microstructure morphology of surfacing alloy layer without adding vanadium element and different manganese content: (a) sample Mn2-V0; (b) sample Mn14-V0

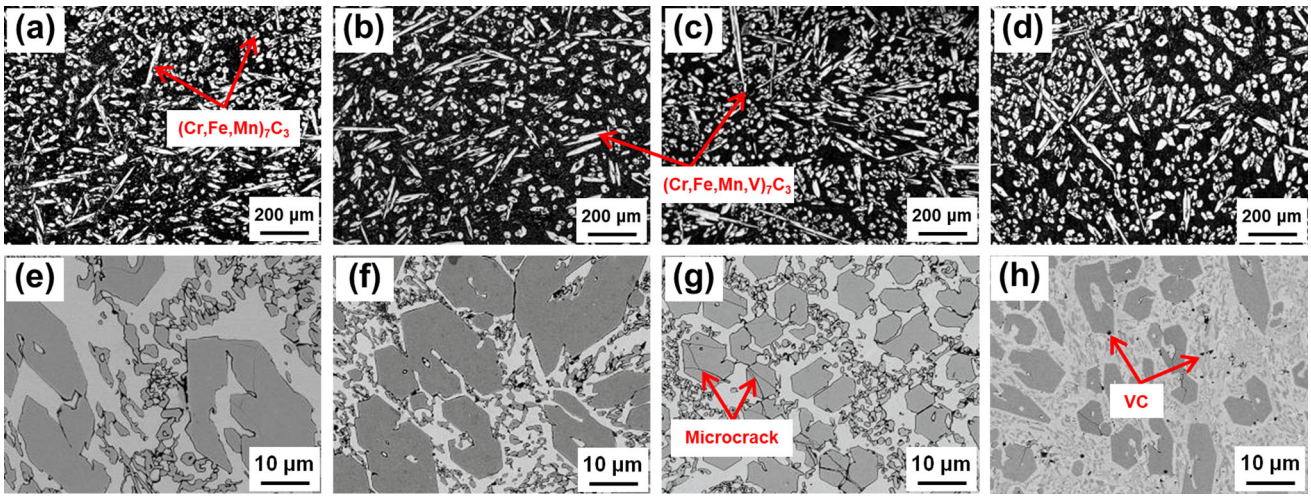

Fig. 4 Microstructure morphology of surfacing alloy layer with different vanadium content: (a, e) sample Mn14-V0, (b, f) sample Mn14-V2, (c, g) sample Mn14-V5, (d, h) sample Mn14-V7

with sizes ranging from 3 to 5 μm. For the sample Mn14-V2, which contains 2.03 wt.% vanadium, the primary carbide M_7C_3 phase exhibits a width of 25-40 μm and a length of about 200 μm. The volume fraction of M_7C_3 in this sample is slightly reduced compared to the vanadium-free sample, accounting for about 50% of the overall structure, while the morphology of the eutectic structure remains unchanged. Increasing the vanadium content further, the Mn14-V5 sample shows a reduction in the size of hexagonal block carbides compared to samples with no or minimal vanadium addition. The width measures approximately 10 μm, and the lengths are predominantly around 100 μm, though some extend to 150-200 μm. The volume fraction of these carbides increases, representing about 70% of the overall structure. When vanadium content reaches 7.11 wt.%, as seen in the sample Mn14-V7, the primary phase size remains relatively unchanged from Mn14-V5, but the volume fraction decreases slightly. Meanwhile, the size of the eutectic small granular carbides refines to about 1 μm. The microstructure also displays the crystallization of second-phase particles. Based on prior studies (Ref 19, 20); it is tentatively suggested that these enhanced second-phase particles are VC, which are small and uniformly dispersed throughout the microstructure. This refinement and dispersion contribute to the improved mechanical properties of the surfacing alloy layer.

Upon analysis, it is evident that the variations in the microstructural morphology of the surfacing alloy layer are contingent upon the vanadium content. When a modest amount of vanadium is introduced, a decrease in primary carbides is observed. Specifically, when the vanadium content remains below 5 wt.%, the eutectic point of the Fe-Cr-C alloy shifts rightward, resulting in reduced crystallization of primary carbides. Conversely, when the vanadium content exceeds 5 wt.%, the eutectic point moves leftward, which facilitates the enhanced crystallization of carbides (Ref 27). Additionally, the increase in the volume fraction and the refinement in size of the primary carbide M_7C_3 are attributed to the presence of VC. Acting as a heterogeneous nucleation core, VC promotes the attachment and crystal growth of primary carbide M_7C_3. This interaction leads to an increase in the volume fraction of the carbides and refinement of the grains. These microstructural changes induced by vanadium addition are crucial for enhancing the mechanical properties and wear resistance of the surfacing alloy layer.

To assess the elemental distribution within the microstructure of the Fe-Cr-Mn-C surfacing alloy, both with and without the addition of vanadium, EDS analyses were conducted. The results are displayed in Fig. 5. Surface and point scanning analyses reveal that Fe predominantly constitutes the matrix

element, accounting for approximately 70 wt.% in the matrix. It is present in smaller proportions in the primary carbide M_7C_3 and the eutectic carbide, with contents of about 20 and 30 wt.%, respectively. The introduction of vanadium does not significantly alter the distribution of Fe within the structure. Cr distribution shows a distinct preference; it primarily contributes to the composition of primary and eutectic carbides and is seldom found dissolved in the matrix. In primary carbides, Cr content can reach as high as 604 wt.%. The addition of vanadium markedly influences the Cr content in the primary carbides, with some vanadium substituting for Cr in both primary and eutectic carbides. At a vanadium content of 7.11 wt.% in the alloy, the Cr content in the primary carbide M_7C_3 of the sample Mn14-V7 decreases to about 40 wt.%, with

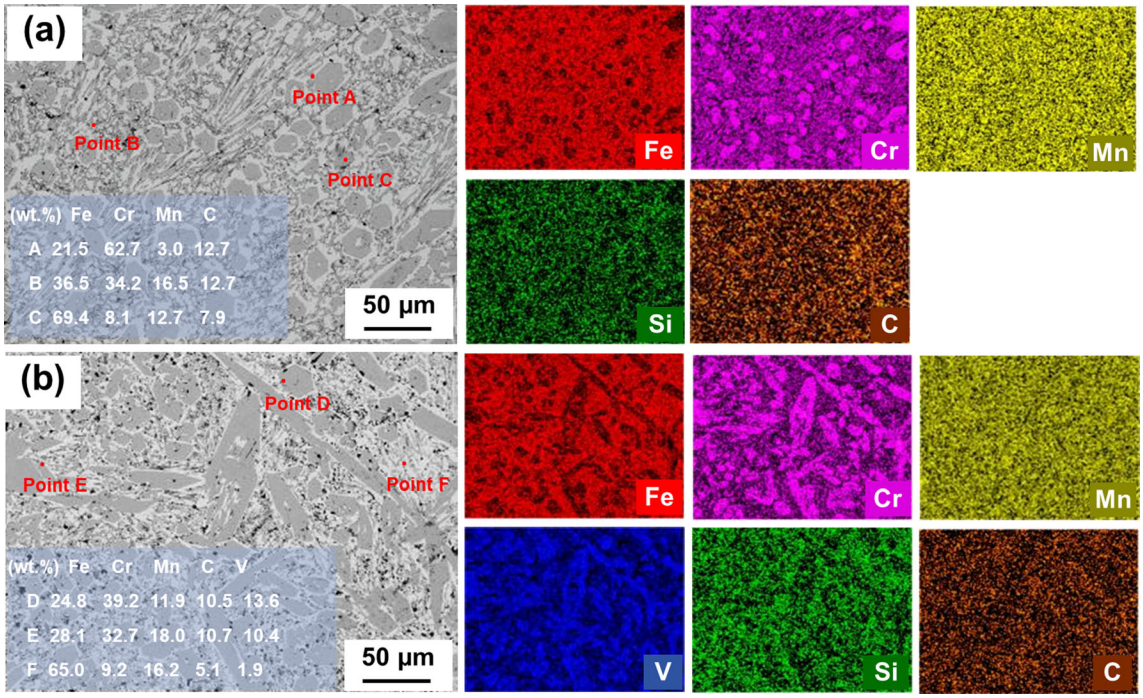

Fig. 5 Element distribution diagram of surfacing alloy layer with different vanadium content: (a) sample Mn14-V0, (b) sample Mn14-V7

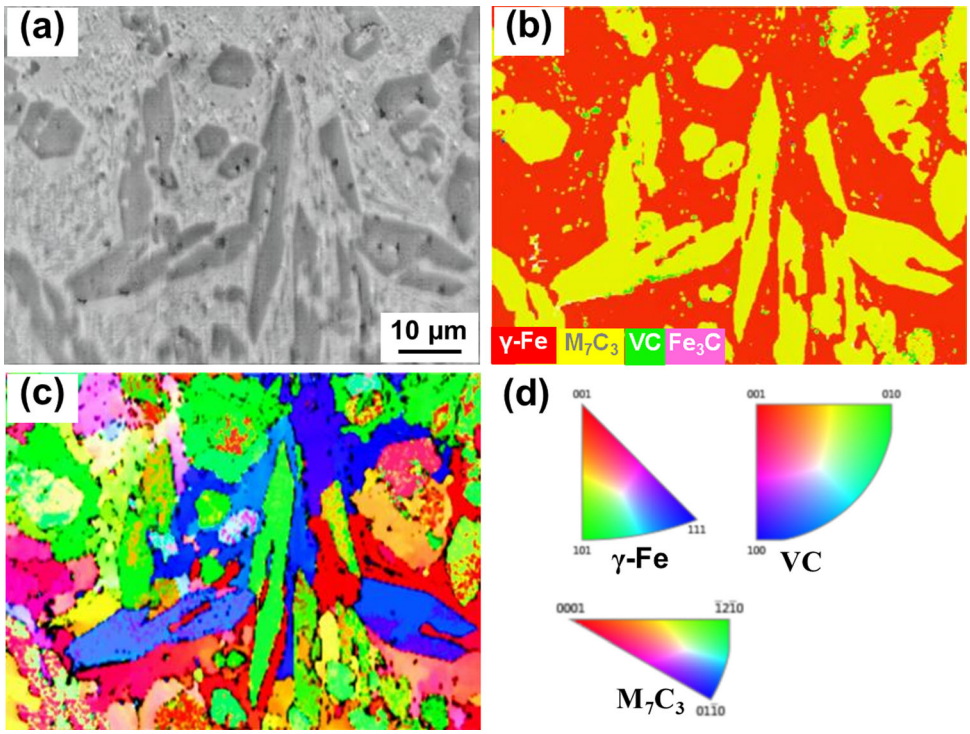

Fig. 6 EBSD analysis of Mn14-V7: (a) SEM image, (b) phase map, (c) IPF-X map, and (d) color-coded map

approximately 10 wt.% of V being incorporated into the primary phase. Mn distribution across the microstructure is relatively uniform, with Mn being present in both the primary and eutectic structures. The addition of vanadium has minimal impact on the distribution of Mn. As an alloying element, vanadium has properties closely resembling those of chromium, readily substituting Cr in the carbide $(Cr, Fe)_7C_3$ and dissolving in M_7C_3 to form solid solution carbides. This substitution alters the lattice structure and properties of the carbides (Ref 28). EDS analysis also highlights another critical role of vanadium: it contributes significantly to the formation of second-phase hard particles, VC, where vanadium content is approximately 60 wt.%. The crystallization of VC particles plays a crucial role in the grain refinement of primary and eutectic carbides, enhancing the overall microstructural stability and wear resistance of the alloy.

To ascertain the composition and growth orientation of phases within the surfacing alloy layer, the sample Mn14-V7 was analyzed using EBSD, with results depicted in Fig. 6. The phase composition map confirms that the orange-red matrix is austenite, which has been completely transformed from its original state by the addition of manganese. The yellow hexagonal block and granular structures identified in the image are primary and eutectic carbides M_7C_3, respectively. The green granular phase interspersed throughout the microstructure is identified as VC, although the small size and low volume fraction of these VC particles results in their absence from XRD detection. VC predominantly forms at the midpoints or edges of M_7C_3 carbides, suggesting that VC crystallizes serve as nucleation cores for M_7C_3 formation, thereby increasing the volume fraction of M_7C_3. Notably, there is almost no crystallization of Fe_3C observed in the phases. The Inverse Pole Figure-X (IPF-X) Map, color-coded for clarity, indicates that the growth orientation of the hexagonal carbide M_7C_3 hard phase is not uniform but occurs in various directions. This staggered distribution of the hard phase plays a crucial role in mitigating the continuous expansion of cracks, thereby positively influencing the fracture toughness and wear resistance of the surfacing alloy layer. This heterogeneous growth orientation and the structural integrity it confers are pivotal in enhancing the performance characteristics of the alloy under operational stresses.

Figure 7 presents the crystallization diagrams of Fe-Cr-Mn-C wear-resistant surfacing alloy layers with varying V content. Fig. 7(a) illustrates the crystallization process in the absence of V addition. As the plasma arc heat source recedes, the temperature of the molten pool decreases, initiating the crystallization of $(Cr, Fe, Mn)_7C_3$ crystal nuclei. With further cooling, these nuclei grow to form a primary $(Cr, Fe, Mn)_7C_3$ hard phase, around which more nuclei crystallize and a eutectic structure of M_7C_3 + Fe develops. Fig. 7(b) describes the crystallization process in the presence of a small amount of V. When the V content is less than 5 wt.%, the eutectic point shifts rightward, inhibiting the formation of primary $(Cr, Fe, Mn)_7C_3$ crystal nuclei, resulting in a decrease in their volume fraction and an increase in their size. Conversely, when the V content exceeds 5 wt.%, the eutectic point moves leftward, enhancing the crystallization of primary phase nuclei. Additionally, the increased V content prompts the crystallization of VC, which acts as a heterogeneous nucleation core. This leads to the refinement of primary carbide M_7C_3 and the hard phase grains. Ultimately, this process results in the formation of a reinforced surfacing alloy structure characterized by a hard phase of $(Cr, Fe, Mn, V)_7C_3$ and VC, with austenite serving as the matrix and featuring smaller grain sizes. This detailed analysis underscores the significant role of vanadium in modulating the microstruc-

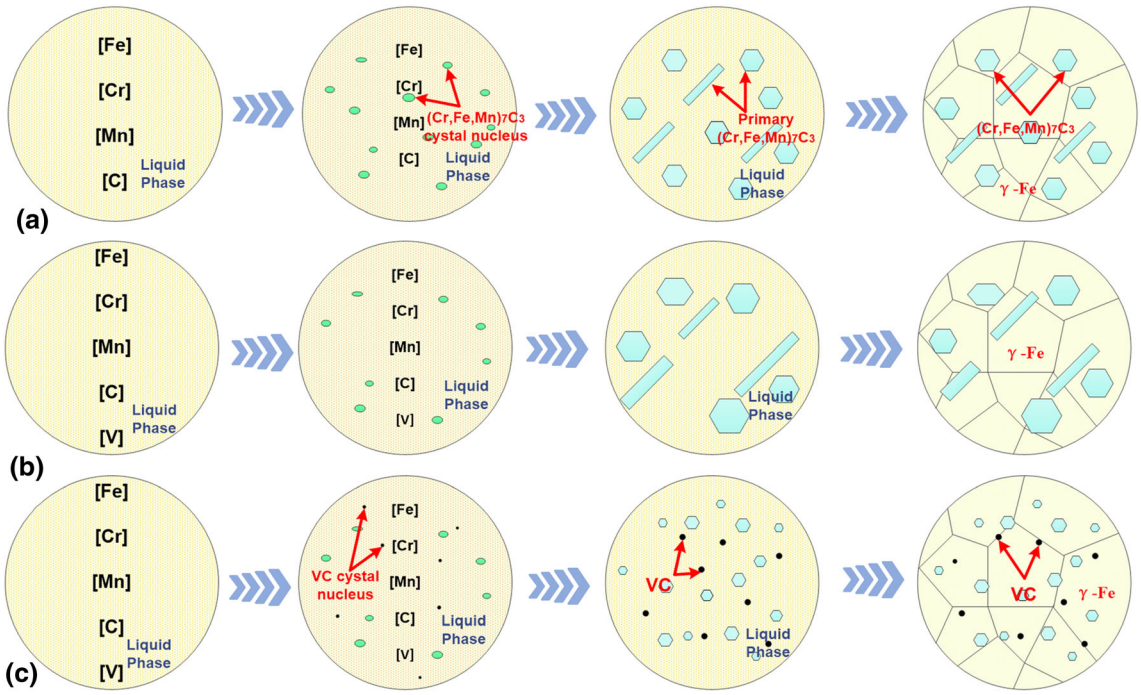

Fig. 7 The schematic diagram of crystallization process of surfacing alloy layer with different manganese and vanadium content: (a) sample Mn14-V0, (b) sample Mn14-V2, (c) sample Mn14-V7

tural characteristics and enhancing the performance of the surfacing alloy layer.

3.3 Impact Fracture Behavior of Surfacing Alloys

Figure 8 depicts the impact toughness values of surfacing alloy layers with varying Mn and V contents. The Mn2-V0 samples, characterized by low Mn content and absence of V, exhibit an impact toughness of 19.80 J/cm^2. This relatively low toughness is primarily due to the hypoeutectic high-chromium cast iron microstructure, which consists of α-Fe dendrites and an α-Fe + M_7C_3 eutectic structure. The matrix toughness of α-Fe is inferior to that of γ-Fe, limiting the potential for high impact toughness. Upon the addition of approximately 20 wt.% Mn to the surfacing alloy layer, the impact toughness increases to 25.20 J/cm^2. This enhancement is attributed to the transformation from a hypoeutectic to a hypereutectic structure, and a consequent change in the matrix phase to austenite. The face-centered cubic lattice structure of austenite provides excellent plasticity, thereby elevating the impact toughness of the surfacing alloy layer. The introduction of V into the surfacing alloy layer initially leads to a reduction in impact toughness, which then increases with further V addition. At a vanadium content of about 2 wt.%, the impact toughness decreases to 19.80 J/cm^2, primarily due to a reduction in the volume fraction of primary carbides and associated strength. However, as the V content increases, the impact toughness values of samples Mn14-V5 and Mn14-V7 rise to 28.10 and 30.00 J/cm^2, respectively, with marginal variation between them. Further increases in V content have a negligible effect on impact toughness. The enhancement in impact toughness with increased V content can be attributed to two main factors. Firstly, when V content exceeds 5 wt.%, the eutectic point shifts leftward, promoting the crystallization and refinement of carbide M_7C_3 and the primary M_7C_3 carbide grains. Secondly, the crystallization of VC particles within the microstructure acts as a secondary reinforcing phase. This refinement of primary carbide grains, coupled with the enhanced strength of the surfacing alloy layer, significantly contributes to the increased impact toughness.

To elucidate the influence of V addition on the fracture mode of the surfacing alloy layer, the SEM morphology of impact fractures in surfacing alloy layers with varying V contents was analyzed. The results are displayed in Fig. 9. Independent of the presence of vanadium, the cross sections of hexagonal rod-shaped primary carbide M_7C_3 are notably smooth, with some sections exhibiting cleavage steps and microcracks. This observation confirms the inherent brittleness of carbide M_7C_3, which predominantly undergoes brittle fracture. Despite this brittleness, the primary carbides possess high hardness, enabling them to withstand significant strength under impact loads. The addition of vanadium significantly alters the fracture mode within the eutectic structure. For instance, in the Mn14-V5 sample, the eutectic structure exhibits a dimple fracture morphology, and some eutectic structures display tearing edges. This fracture pattern indicates a mix of brittle and ductile fracture characteristics. The ductile fracture mode within the eutectic structure is primarily associated with the transformation of the matrix to austenite and the grain refinement of small block eutectic carbides. These changes contribute to the enhanced toughness of the eutectic phase, reflecting the complex interplay between microstructural evolution and mechanical properties induced by vanadium addition.

3.4 Wear Resistance and Wear Mechanism of Surfacing Alloys

Figure 10 presents the Rockwell hardness and wear weight loss characteristics of surfacing alloy layers with varying contents of Mn and V. In the Mn2-V0 sample, where V is absent and Mn content is low, the Rockwell hardness registers at 50.1 HRC, indicating relatively low hardness. As the Mn

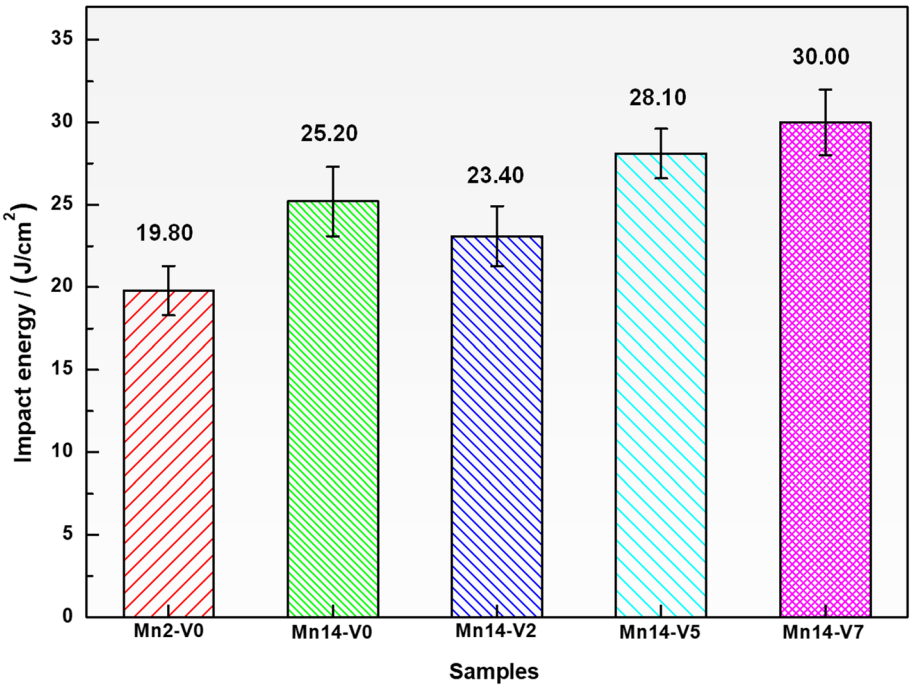

Fig. 8 Impact toughness value of surfacing alloy layer with different manganese and vanadium content

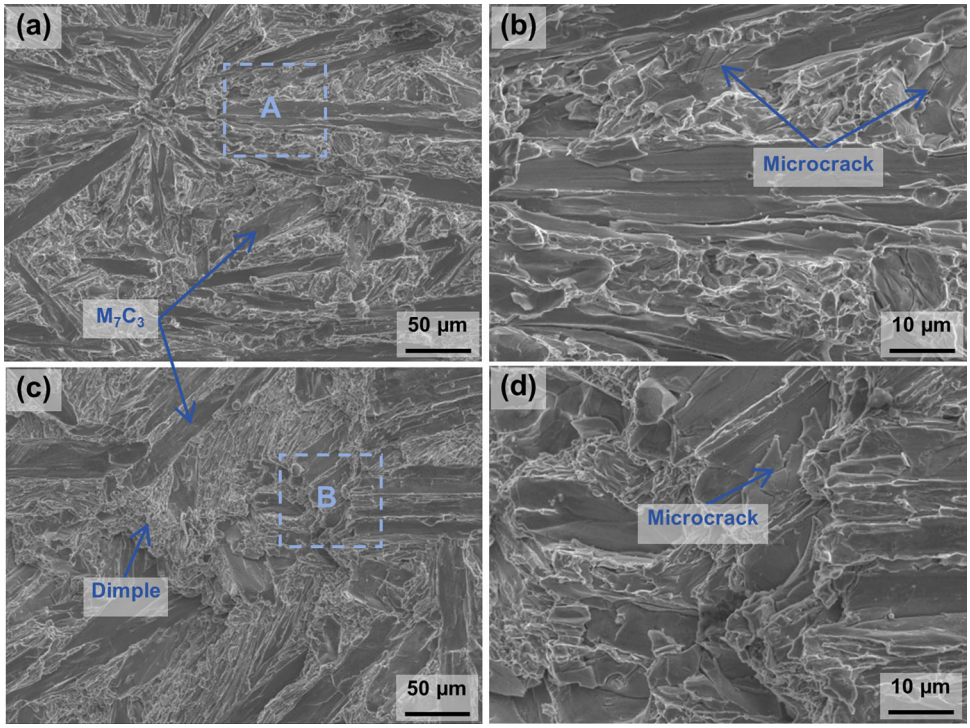

Fig. 9 Microscopic fracture of surfacing alloy layer with different vanadium addition contents: (a) sample Mn14-V0, (b) A region enlargement diagram, (c) sample Mn14-V5, (d) B region enlargement diagram

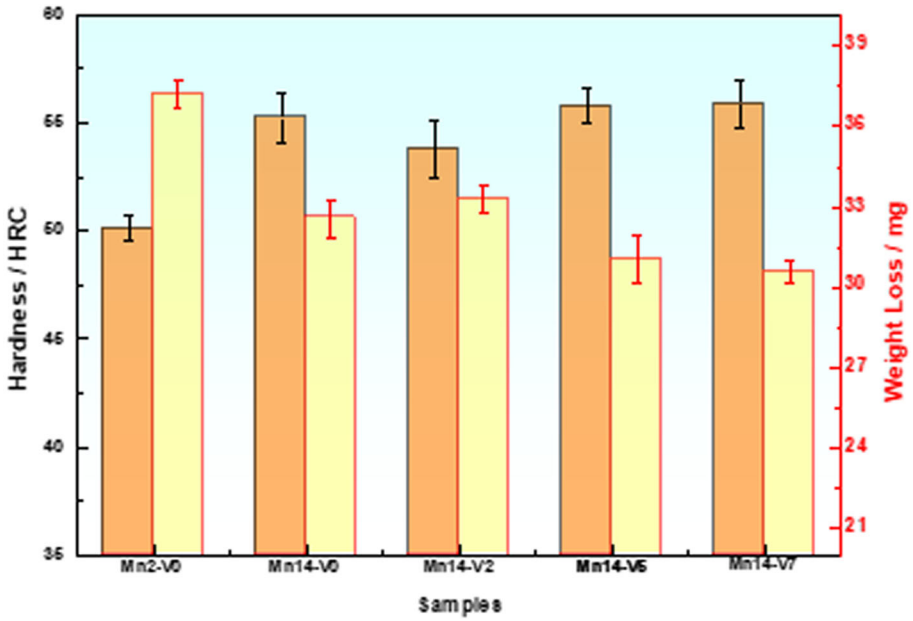

Fig. 10 Rockwell hardness and wear weight loss diagram of surfacing alloy layers with different manganese and vanadium contents

content is increased within the surfacing alloy layer, the structure transitions from hypoeutectic to hypereutectic. This transformation results in the crystallization of a substantial quantity of high-hardness M_7C_3 carbides, significantly enhancing the hardness to 55.2 HRC for the Mn14-V0 sample. With the incremental addition of V, the hardness of the surfacing alloy layer initially decreases and then increases. The Rockwell hardness for the Mn14-V2 sample is measured at 53.8 HRC, primarily due to a reduction in the volume fraction of primary carbides. The hardness of the surfacing alloy layer is directly proportional to the volume fraction of the hard phase; a higher volume fraction of hard phases correlates with increased hardness (Ref 29). As the V content further increases, the hardness of the surfacing alloy layer also rises. The Rockwell hardness for the Mn14-V5 and Mn14-V7 samples reaches 55.8 and 55.9 HRC, respectively. This increase in hardness is

attributed to the enhanced crystallization of hard carbides and the secondary reinforcing phase of VC particles. The presence of V promotes these crystallizations, crucially contributing to the hardness increase. However, significantly higher increments of V content do not substantially increase the hardness but rather lead to increased production costs of the surfacing alloy layer.

The wear resistance of the surfacing alloy layer exhibits a trend similar to that of its hardness changes. The addition of Mn enhances the wear resistance of the surfacing alloy layer. However, with the incorporation of V, the wear resistance initially decreases and then increases. The sample Mn2-V0, with no added V and low Mn content, shows a wear weight loss of 37.20 mg under a load pressure of 24 N, reflecting the inferior wear resistance of hypoeutectic high-chromium cast iron surfacing alloy layers. As the Mn content is increased, transforming the alloy into a hypereutectic high-chromium cast iron, a significant crystallization of high-hardness M_7C_3 carbides occurs within the structure. These hard phases are effective in resisting the indentation of abrasive particles, thereby markedly improving wear resistance. For instance, the wear weight loss for the sample Mn14-V2 is 32.57 mg. However, the addition of a small amount of V slightly reduces wear resistance due to the inhibition of primary phase carbides' crystallization, as evidenced by the wear weight loss of 33.30 mg for Mn14-V2. Further increases in V content to levels in Mn14-V5 and Mn14-V7 lead to wear weight losses of 31.05 and 30.60 mg, respectively, under the same load pressure. This improvement in wear resistance is attributable to the increased volume fraction of primary carbide M_7C_3 and enhanced microhardness. Additionally, the crystallization of second-phase reinforcing particles, such as VC, plays a crucial role in the continued enhancement of wear resistance. However, excessively increasing the V content does not significantly further improve wear resistance but rather adds to the cost of the surfacing alloy layer. Therefore, optimizing the addition of V within the surfacing alloy layer is essential to balance performance improvement with cost-effectiveness.

Figure 11 displays the two-body abrasive wear surface morphology of Fe-Cr-Mn-C wear-resistant surfacing alloy layers with varying V contents. As depicted in Fig. 11(a), the wear surface of the Mn14-V0 sample, which lacks V addition, exhibits numerous deep and wide furrows. This surface morphology arises because the volume fraction of primary carbides within the surfacing alloy layer is low. Consequently, when abrasive particles traverse this surface, the sparse distribution of hard phases struggles to resist the indentation caused by these particles. During the rotation of the turntable, the abrasive particles induce lateral slippage against the surface of the sample, leading to the formation of furrows. Additionally, several spalling pits are evident on the surface. This spalling occurs because the hard phase M_7C_3 is inherently brittle; when abrasive particles impact this brittle block structure, it tends to fracture and spall. The predominant wear mode observed for this sample involves microcutting, with microfracture playing a secondary role. This characterization underscores the critical influence of hard phase density and composition in determining the wear resistance of surfacing alloys.

The addition of a small amount of V to the surfacing alloy layer influences the wear characteristics significantly, as observed in the Mn14-V2 sample. This sample exhibits deeper and wider furrows on its worn surface compared to the Mn14-V0 sample, which does not contain V. Additionally, the spalling

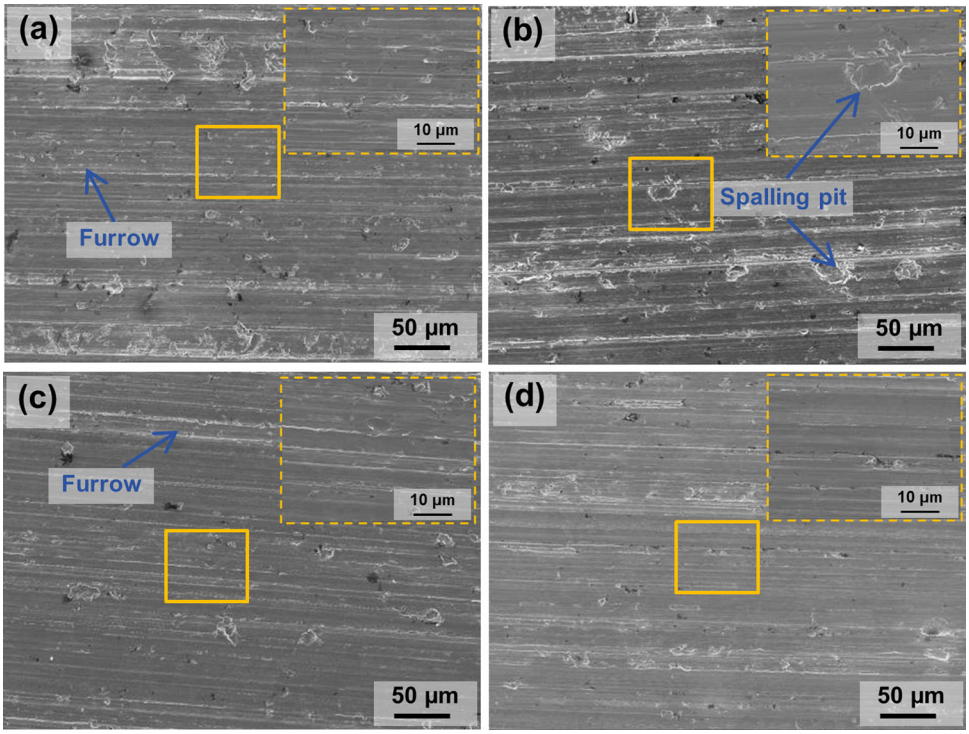

Fig. 11 SEM morphology of two-body wear of surfacing alloy layer with different chromium contents under 24 N contact load: (a) sample Mn14-V0, (b) sample Mn14-V2, (c) sample Mn14-V5, (d) sample Mn14-V7

pits on the Mn14-V2 sample are larger and more prevalent. This increased wear damage can be attributed to the influence of vanadium, which inhibits the crystallization of primary carbides in the surfacing alloy layer and results in larger M_7C_3 carbides. The reduced volume fraction of the hard phase due to the presence of vanadium makes it more challenging for the material to resist the abrasive action of the particles, leading to more pronounced furrows on the sample surface. As the size of the M_7C_3 carbides increases, so does the size of the brittle fracture spalling, enlarging the spalling pits and consequently increasing the wear weight loss. The wear mode observed in the Mn14-V2 sample predominantly features a combination of microfracture and microcutting, which are characteristic of the deleterious impact of reduced carbide crystallization and increased carbide size due to vanadium addition. This highlights the complex trade-offs in alloy composition adjustments for optimizing wear resistance in surfacing alloys.

With an increased V content in the surfacing alloy layer, as depicted in Fig. 11(c) and (d), notable reductions are observed in the depth and width of the plow grooves on the surface of the sample, along with a significant decrease in both the proportion and size of peeling pits. When the V content exceeds 5 wt.%, there is an enhanced crystallization of the hard phase within the surfacing alloy layer, and the primary carbide M_7C_3 is notably refined. This refinement leads to an increase in the number of small particles within the eutectic structure, contributing to an overall structural refinement. The hexagonal close-packed structure of primary M_7C_3 carbides exhibits improved resistance to the indentation caused by abrasive particles. Additionally, the refined small block eutectic structure effectively supports the hard phase, helping to prevent fragmentation and spalling. This effective synergy results in excellent wear resistance of the surfacing alloy layer. With a substantial addition of V, a large number of VC particles known for their high hardness are crystallization throughout the microstructure. These particles, in conjunction with the primary carbide M_7C_3, significantly enhance the wear resistance of the surfacing alloy layer. After the inclusion of V, the predominant wear mode of the sample shifts to microcutting, with a minor component of microfracture wear. This change underscores the influence of V in modifying the wear characteristics by strengthening the microstructure and optimizing the resistance to abrasive forces.

Figure 12 presents a physical model illustrating the wear morphology of surfacing alloy layers with varying additions of V. In the samples without V, as abrasive particles traverse the surface under load, they are pressed into the surfacing layer due to the normal force and propelled forward by the tangential force, resulting in the formation of furrows on the surface. The brittle hard phase $(Cr, Fe, Mn)_7C_3$ within these layers tends to fracture and peel off under the abrasive stress, leading to severe wear. Upon the addition of V, the crystallization of the primary phase crystal nuclei is enhanced, increasing the volume fraction and effectively refining the grain structure. This refinement improves the toughness of the hard phase, which becomes less prone to fracturing under the action of abrasive particles. Consequently, the formation of spalling pits is reduced, significantly enhancing the wear resistance of the surfacing layer. This model demonstrates how the strategic incorporation of V into the alloy composition not only alters the microstructural dynamics but also significantly improves the overall wear performance of the surfacing alloy layer.

4. Conclusion

(1) The addition of Mn and V significantly alters the phase composition and morphology of the surfacing alloy layer. Initially, the sample containing no added V and only a small amount of Mn displays characteristics of a typical hypoeutectic high-chromium cast iron. Subsequently, with the incorporation of approximately 14 wt.% Mn, the alloy transitions into a hypereutectic structure, and the matrix phase converts into austenite. Further modification involves the addition of a minor quantity of V, which preferentially dissolves in the primary carbide M_7C_3, subsequently inhibiting its crystallization. However, when the V content exceeds 4.60 wt.%, there is a promotion in the crystallization of the primary phase M_7C_3. Concurrently, the secondary hard particle phase VC is formed, effectively refining the grains of primary M_7C_3. This complex interaction between Mn and V additions thus plays a crucial role in optimizing the microstructural properties of the surfacing alloy, enhancing its overall performance characteristics.

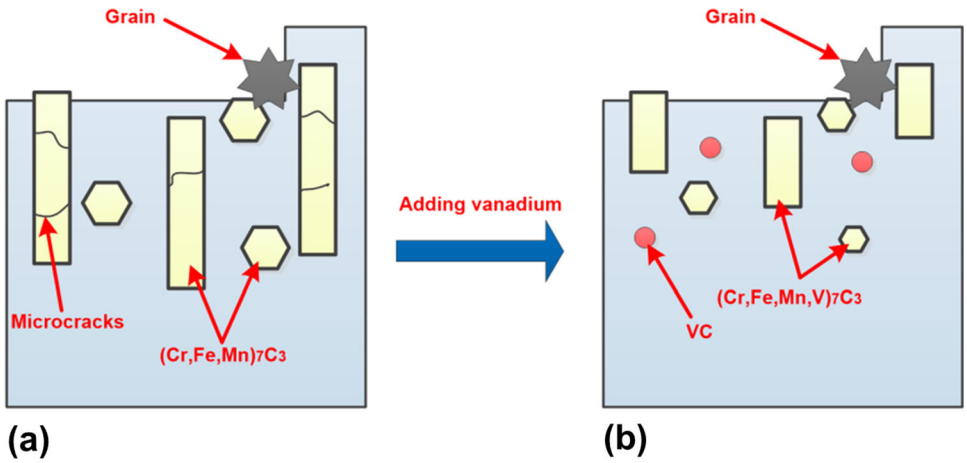

Fig. 12 Physical model of wear morphology of surfacing alloy layer with different manganese and vanadium content: (a) sample Mn14-V0, (b) sample Mn14-V7

(2) The incorporation of Mn and V elements notably enhances the impact toughness of the surfacing alloy layer. Initially, the Mn2-V0 sample, which contains no added V and a low content of Mn, exhibits an impact toughness value of 19.80 J/cm^2. The subsequent addition of Mn significantly boosts the impact toughness, with the Mn14-V0 sample achieving a value of 25.20 J/cm^2. Further modification by adding V initially results in a decrease in impact toughness, which then progressively increases with higher V concentrations. Although the improvement in impact toughness with increased V content is modest, it is significant; the sample Mn14-V7, which contains a higher amount of V, reaches an impact toughness of up to 30.00 J/cm^2. This pattern underscores the nuanced role of V in modulating the mechanical properties of the surfacing alloy, optimizing its resistance to impact through careful compositional adjustments.

(3) The addition of Mn and V significantly enhances the hardness and wear resistance of the surfacing alloy layer. Initially, the sample Mn2-V0, which contains no V and a low Mn content, demonstrates suboptimal hardness and wear resistance, with a hardness of only 50.1 HRC and a wear weight loss of 37.2 mg. Subsequent incorporation of Mn into the alloy leads to noticeable improvements in both hardness and wear resistance. The introduction of V further influences these properties, exhibiting a trend where both hardness and wear resistance initially decrease and then increase. Notably, the sample Mn14-V7 showcases the most superior performance among the tested samples. It achieves a high hardness of 55.9 HRC and a reduced wear weight loss of 30.6 mg, indicating the beneficial effects of optimized Mn and V additions in enhancing the overall performance of the surfacing alloy layer.

Acknowledgments

The work was supported by the Heilongjiang Province Natural Science Foundation, China [LH2023E023]; Heilongjiang Provincial Colleges and Universities Basic Scientific Research Business Fee Outstanding Innovation Team Construction Project, China [2023-KYYWF-0637]; National Natural Science Foundation of China [52101222]; and the Jiamusi University National Fund Cultivation Project [JMSUGPZR2023-009].

References

1. A.S. Kang, G. Singh, and G.S. Cheema, Improving Wear Resistance via Hardfacing of Cultivator Shovel, *Mater. Today Proc.*, 2017, **4**(8), p 7991–7999.
2. A. Sharma, A. Kumar, and R. Tyagi, Erosive Wear Analysis of Medium Carbon Dual Phase Steel under Dry Ambient Condition, *Wear*, 2015, **334**, p 33591–33598.
3. W.X. Wang, F. Salvatore, J. Rech, and J.Y. Li, Investigating Effects of Adhesion Wear on Cutting Efficiency and Energy Cost in Dry Belt Finishing, *Int. J. Adv. Manuf. Technol.*, 2018, **95**, p 2119–2123.
4. T. Yue and M.W. Abdel, Finite Element Analysis of Fretting Wear under Variable Coefficient of Friction and Different Contact Regimes, *Tribol. Int.. Int.*, 2017, **107**, p 274–282.
5. H. Sabet, S. Khierandish, S. Mirdamadi, and M. Goodarzi, The Microstructure and Abrasive Wear Resistance of Fe-Cr-C Hardfacing Alloys with the Composition of Hypoeutectic, Eutectic, and Hypereutectic at Cr/C6, *Tribol. Lett.. Lett.*, 2011, **44**, p 237–245.
6. R.P. Rauta, S.F. Rodrigues, V.S. Leal, G.S. Reis, C. Aranas, and V.A. Ferraresi, Influence of Pushing and Pulling the Electrode Procedure and Addition of Second Layer of Welding on the Wear in Hardfacing of Fe-Cr-C, *Mater. Res.*, 2016, **19**, p 1193–1200.
7. E.O. Correa, N.G. Alcântara, L.C. Valeriano, N.D. Barbedo, and R.R. Chaves, The Effect of Microstructure on Abrasive Wear of a Fe-Cr-C-Nb Hardfacing Alloy Deposited by the Open Arc Welding Process, *Surf. Coat. Technol.*, 2015, **276**, p 479–484.
8. S. Buytoz, Microstructural Properties of M_7C_3 Eutectic Carbides in a Fe-Cr-C alloy, *Mater. Lett.*, 2006, **60**, p 605–608.
9. Y. Li, P.X. Zhu, C. Tang, and Z. Sun, Effects of Quenching Medium on Microstructure and Mechanical Properties of High Chromium Cast Iron, *Crystals*, 2022, **12**, p 1332.
10. Y. Wu, L.S. Ma, X.L. Zhou, Y.H. Duan, L. Shen, and M.J. Peng, Insights to Electronic Structures, Elastic Properties, Fracture Toughness, and Thermal Properties of $M_{23}C_6$ Carbides, *Int. J. Refract. Metals Hard Mater.*, 2022, **109**, p 105985.
11. Y. Tian, H.G. Fu, J. Lin, X.Y. Guo, and Y.P. Lei, Microstructure and Properties of Casting Fe-Cr-B Alloy After Quenching Treatment, *Trans. Indian Inst. Met.*, 2019, **72**(7), p 1823–1835.
12. Y.C. Li, P. Li, K. Wang, H.Z. Li, M.Y. Gong, and W.P. Tong, Microstructure and Mechanical Properties of a Mo Alloyed High Chromium Cast Iron After Different Heat Treatments, *Vacuum*, 2018, **156**, p 59–67.
13. Z. Ma, Y.H. Zhang, L.T. Mu, Z.Q. Huang, K.X. Di, J.H. Su, M.H. Zhuang, S.D. Yuan, and L.Q. Wang, Effects of Mo Alloying on the Microstructure and Wear Resistance of Fe-B Surfacing Alloys, *J. Mater. Res. Technol.*, 2023, **23**, p 6162–6175.
14. C.L. Zhang, S.H. Li, Y.H. Lin, J. Jiang, and H.G. Fu, Effect of Boron on Microstructure Evolution and Properties of Wear-Resistant Cast Fe-Si-Mn-Cr-B Alloy, *Mater. Res. Technol.*, 2020, **9**(3), p 5564–5576.
15. Z.H. Guo, F.R. Xiao, S.L. Lu, H.Y. Li, and B. Liao, Effects of Heat-Treatment on the Microstructure and Wear Resistance of a High-Chromium Cast Iron for Rolls, *Adv. Mater. Sci. Eng.*, 2016, **2016**, p 1–7.
16. L.Q. Gong, H.G. Fu, and X.H. Zhi, Microstructure and Properties of Cu-Bearing Hypereutectic High Chromium Cast Iron, *Mater CharactCharact*, 2023, **195**, p 112546.
17. D. Liu, R. Liu, and Y. Wei, Effects of Titanium Additive on Microstructure and Wear Performance of Iron-Based Slag-Free Self-Shielded Flux-Cored Wire, *Surf. Coat. Technol.*, 2012, **207**, p 579–586.
18. N. Shigenori, K. Tadashi, and M. Hideto, Influence of Melting Conditions on Morphology of Vanadium-Carbide in Stainless Spheroidal Carbide Cast Iron, *J. Jpn. Foundry Eng. Soc.*, 2007, **79**, p 133.
19. V. Efremenko, K. Shimizu, T. Pastukhova, Y. Chabak, M. Brykov, K. Kusumoto, and A. Efremenko, Three-Body Abrasive Wear Behaviour of Metastable Spheroidal Carbide Cast Irons with Different Chromium Contents, *Int. J. Mater. Res.*, 2018, **109**(2), p 147–156.
20. W.Q. Leng, L.J. Xu, T. Jiang, X.D. Wang, S.Z. Wei, X.W. Shi, and M. Li, Carbide and Matrix Microstrure Evolution of High-Vanadium Wear-Resistance Cast Iron with High-Silicon Content During Austempering, *Int. J. Metal. Cast.*, 2023, **17**, p 1859–1870.
21. V.G. Efremenko, K. Shimizu, A.P. Cheiliakh, T.V. Kozarevskaya, K. Kusumoto, and K. Yamamoto, Effect of Vanadium and Chromium on the Microstructural Features of V-Cr-Mn-Ni Spheroidal Carbide Cast Irons, *Int. J. Miner. Metall. Mater.*, 2014, **21**(11), p 1096–1108.
22. Q.C. Liu, M.H. Zhuang, Z. Ma, X.X. Li, S.D. Yuan, X.Y. Liu, and P. Lv, Microstructure and Two-Body Abrasive Wear Mechanism of the Fe-3.9 wt% B Wear-Resistant Overlay Alloy with Different Manganese Contents, *Mater. Today. Commun.*, 2023, **35**, p 105865.
23. Y.X. Jian, Z.F. Huang, J.D. Xing, X.T. Liu, L. Sun, B.C. Zheng, and Y. Wang, Investigation on Two-Body Abrasive Wear Behavior and Mechanism of Fe-3.0 wt% B Cast Alloy with Different Chromium Content, *Wear*, 2016, **362**, p 68–77.
24. K. Ono, K. Adachi, I. Miyamoto, and T. Inoue, Influence of Oxide Film on Weld Characteristics of Mild Steel in CO_2 Laser Welding, *J. Laser Appl.*, 2002, **14**, p 73–77.
25. T. Liu, J.B. Sun, Z.X. Xiao, J. He, W.D. Shi, and C.X. Cui, Effect of Multi-element Microalloying on the Structure and Properties of High Chromium Cast Iron, *Materials*, 2023, **16**(9), p 3292.
26. A. Hadji, K. Bouhamla, and H. Maouche, Improving Wear Properties of High-Chromium Cast Iron by Manganese Alloying, *Int. J. Metalcast.Metalcast.*, 2016, **10**, p 43–55.

27. X. Qi, Z. Jia, Q. Yang, and Y. Yang, Effects of Vanadium Additive on Structure Property and Tribological Performance of High Chromium Cast Iron Hardfacing Metal, *Surf. Coat. Technol.*, 2011, **205**, p 5510–5514.
28. A. Sánchez, A. Bedolla-Jacuinde, F.V. Guerra, and I. Mejía, Vanadium Additions to a High-Cr White Iron and Its Effects on the Abrasive Wear Behavior, *Materials*, 2020, **414**, p 3077–3089.
29. X. Chong, M. Hu, P. Wu, Q. Shan, Y. Jiang, Z. Li, and J. Feng, Tailoring the Anisotropicmechanical Properties of Hexagonal M_7X_3 (M¼Fe, Cr, W, Mo, X¼C, B) Bymultialloying, *Acta Mater. Mater.*, 2019, **169**, p 193–208.